Plasma-induced spatiotemporal modulation of propagating femtosecond pulses

Litao Ding (丁立涛), Juan Song (宋 娟), Zhenrong Sun (孙真荣), Li Deng (邓 莉), and Zugeng Wang (王祖赓)

Key Laboratory of Optical and Magnetic Resonance Spectroscopy (East China Normal University), Ministry of Education, and Department of Physics, East China Normal University, Shanghai 200062

Received May 9, 2006

The dynamics of the femtosecond pulse propagation in a plasma channel is investigated by the pump-probe longitudinal diffractometry and second harmonic generation frequency-resolved optical gating (SHG-FROG) technique. The spatial characteristics, corresponding to the electronic density and the size of the channel, can be observed by the recorded ring pattern, and the spectral and temporal characteristics are recorded by the SHG-FROG traces. The spatiotemporal characteristics will help us to better understand the dynamics of the plasma induced by the femtosecond pulse and the femtosecond pulse propagating in the plasma channel.

OCIS codes: 350.5400, 320.2250, 060.5060, 190.2640.

Propagation of femtosecond pulses in plasma has been extensively studied during the last decade. The propagation of intense femtosecond laser pulses in gases and plasmas is relevant to a wide range of applications, including laser-driven accelerators[1−3], laser-plasma channeling[4,5], harmonic generation[6,7], supercontinuum generation[8], X-ray lasers[9,10], and so on. The propagating dynamics of the femtosecond laser pulses in plasma is important for fundamental physics, particle acceleration and fast igniter projects[11,12]. The investigations on the laser-induced plasma are of fundamental importance for guiding optical pulses in the plasma waveguides and have been extensively reported[13−15]. When the femtosecond laser pulses propagate in the plasma channel, self-phase modulation, caused by temporal variation in the plasma refractive index, can induce observable spectral modulation of the propagating laser pulses. The line-shape of the blue-shifted spectrum is a sensitive function of the time-dependent electron density, and so it can be used to characterize the plasma. Recently, plasma-induced spectral and spatial distortions of the propagating femtosecond pulses are studied by two-color pump-probe spectroscopy[16]. However, its time resolution is limited by the duration of the probe pulses. So, the recently developed frequency-resolved optical gating (FROG) technique with the resolution of a few femtoseconds provides an absolute time reference, and enables simultaneous monitoring of the amplitude and phase of the propagating femtosecond pulses. It has been used to examine high-intensity pulse propagation in the aluminum plasma[17], and the femtosecond pulse propagation in the preformed plasma channels[18]. In this paper, the pump-probe longitudinal diffractometry and second harmonic generation FROG (SHG-FROG) technique are employed to characterize the spatiotemporal properties of the femtosecond pulses propagating in the laser-induced plasma channel.

The layout of our experimental setup is shown in Fig. 1. A Ti:sapphire mode-locked laser (Spectra-Physics Spitfire amplifier) is used as the excitation source with the pulse width of 50 fs, the repetition rate of 1 kHz, and the center wavelength of 800 nm. The total energy of the laser is about 700 μJ, the beam profile is nearly Gaussian with a beam waist of 7 mm. The laser beam is split into pump and probe beams. The pump beam ($\sim$ 500 μJ) is introduced into an adjustable delay line and focused into a carbon bisulfide sample cell with the thickness of 50 mm by a lens with the focal length of 400 mm, and the full-width at half-maximum (FWHM) at focus in vacuum is about 50 μm. A variable attenuator is employed to adjust the pump pulse energy. The probe beam is attenuated to less than 10 μJ, and then is focused by a lens with the focal length of 400 mm into the plasma channel in the opposite direction. The photograph of the diffraction pattern in a white screen, placed at the distance of 50 cm after the cell, is taken with a charge-coupled device (CCD) camera. In order to investigate the pulse propagation, SHG-FROG technique has been employed to characterize the femtosecond pulses propagating in the laser-induced plasma.

In the medium or plasma, the pulse propagation depends on diffraction, refraction, ionization, nonlinear self-focusing, and defocusing. In an unionized medium and for laser power $P < P_{\rm cr}$ ($P_{\rm cr}$ is the critical ionization power), the refractive index is given by $n_{\rm r} \simeq n_0 + n_2 I$, where n_0 is the linear refraction, n_2 the nonlinear refraction, and I the laser intensity. However, when $P > P_{\rm cr}$, the pulse self-focusing and the increasing peak intensity

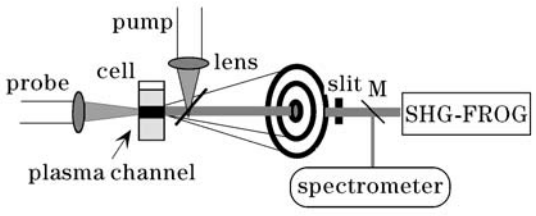

Fig. 1. Experimental setup for measuring the evolution of the probe pulses propagating in the plasma channel.

result in multi-photon ionization, and then the plasma channel will be formed. As a result, electrons (rather than ions) are expelled from the axis into the area of the weak field by the pondermotive force[14], which is a spatial gradient force of the laser field with the field intensity of E^2 and takes the form of $f_{\rm NL} = -\frac{q^2}{4m\omega_2}E(x)^2$, where ω is the laser frequency, m and q are the quality and electric quantity of the electrferous particle, respectively. Since the laser intensity in the ionization channel has a radial gradient, the electron density in the plasma channel caused by the multi-photon ionization will have also a radial gradient. In the region of the plasma, the refractive index is modified as[13]

$$n_{\rm r} \simeq n_0 + n_2 I - \omega_{\rm p}^2(r)/2\omega^2, \tag{1}$$

where $\omega_{\rm p} = (4\pi e^2 N_{\rm e}/m)^{1/2}$ is the plasma frequency, $\omega = ck$ is the laser frequency, c the velocity of light, k the wave vector, $N_{\rm e}(r)$ is the electron density in the plasma and can be normalized by the equilibrium density N_0[19],

$$N_{\rm e}(r) = 1 + (\frac{{\rm d}^2}{{\rm d}r^2} + \frac{1}{r}\frac{\rm d}{{\rm d}r})\sqrt{1+A^2}, \tag{2}$$

where $A(r)$ is the normalized pump intensity with a Gaussian-like transverse profile. The profile of the electron density in the transverse dimension is shown in Fig. 2. A minimum electron density at $r = 0$ can be observed, and a great gradient is formed with a normalized pump intensity at 2.5 due to the pondermotive force. When the normalized pump intensity is increased to 5.5, it is obvious that the electron gradient is steeper and the electronic density at $r = 0$ has a great decrease. The electron density gradient results in the refraction gradient, and so the probe beam will be focused and guided when it propagates through this plasma channel[13]. The model of total refraction can be employed to explain the plasma focusing. When the probe beam propagates in this channel, the diffraction and total refraction can confine the beam in the channel. The more beam energy will be guided with increasing the electron density gradient due to predominant total refraction.

The measured spot size and transmitted energy of the probe beam at a 50-cm distance out of the cell are recorded, as shown in Fig. 3. When the pump energy is

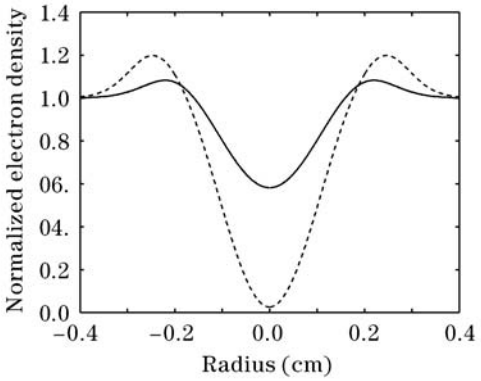

Fig. 2. Theoretical fitting for the transverse electron density (normalized by the equilibrium density N_0) profile at normalized pump intensities of 2.5 (solid line) and 5.5 (dashed line).

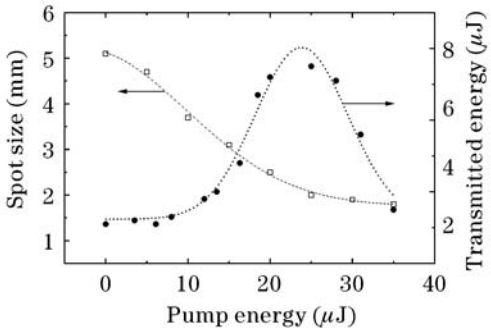

Fig. 3. Spot size and transmitted energy of the probe beam as functions of the pump energy.

increased from 0 to 30 μJ, the diameter of the spot decreases from 5.1 to 1.8 mm due to plasma focusing, meanwhile the transmitted probe energy rapidly increases to 7.5 μJ when the pump energy is 20 μJ and then greatly decreases when the pump energy increases between 25—35 μJ. As well known, the plasma channel can be formed when the peak intensity of the pump beam is larger than the critical ionization power, and the generated plasma lens focuses and guides the probe beam in a small spot size. When the stronger pump energy is injected into the plasma channel, the higher plasma density gradient results in the decrease of focal length of the plasma-lens, and the higher energy probe beam is guided. However, when the pump power is increased to 25 μJ, the multi-ionization channel is formed because of various instabilities such as Raman processes and laser-envelope modulations[19], and then the break up of the probe pulse in space will be produced. So, the probe pulse is greatly scattered in the process of propagating through this multi-ionization channel, and it results in the decrease of the transmitted probe energy.

A probe beam with a Gaussian-like transverse profile, propagating in a plasma channel, will experience a spatiotemporal self phase modulation. Self phase modulation in the transverse profile can induce the formation of the diffractive ring, and self phase modulation in temporal domain can cause the spectral broadening. If the phase increment $[\Delta\phi]_{\rm max}$ is much larger than 2π, the

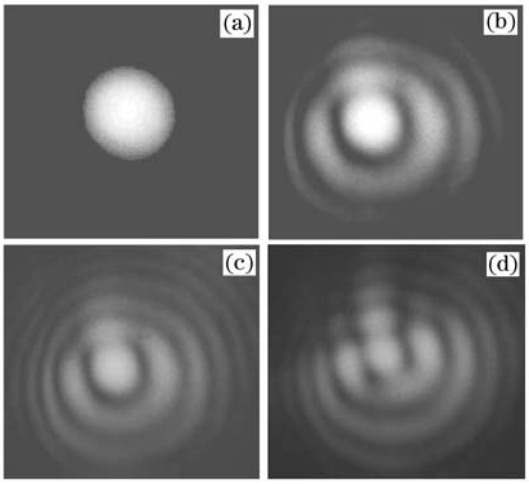

Fig. 4. Recorded fringe patterns at the pump energies of 0 (a), 10 (b), 20 (c), and 35 μJ (d).

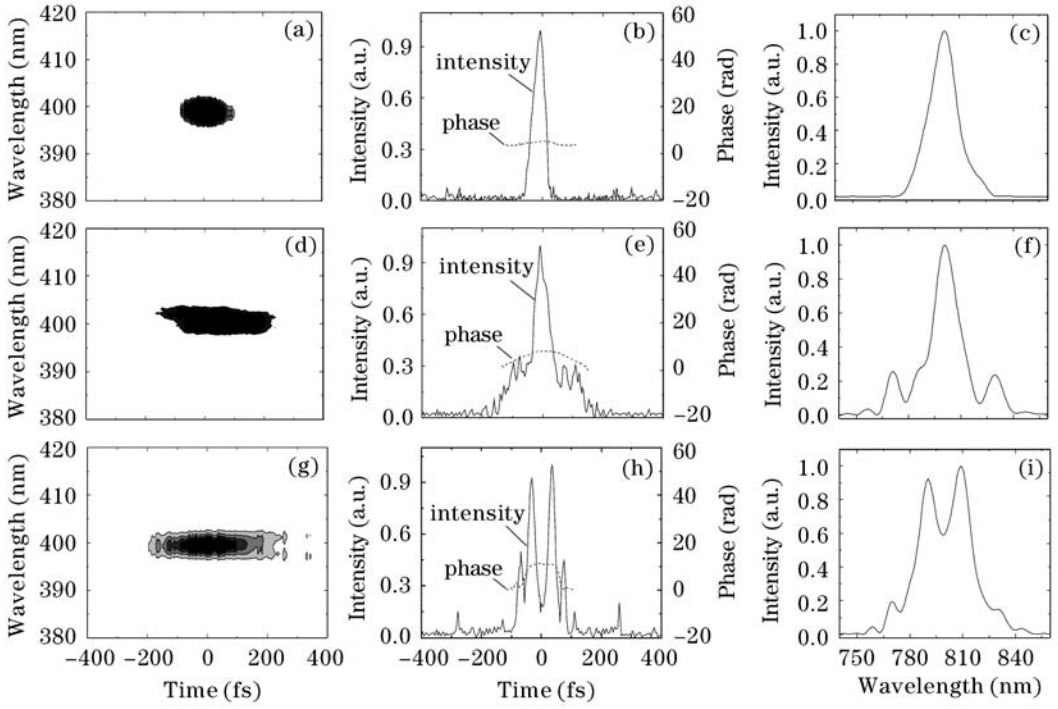

Fig. 5. SHG-FROG traces, retrieved envelope phase traces, and power spectra for the probe beam at the pump energies of 0 ((a)—(c)), 10 ((d)—(f)), and 20 μJ ((g)—(i)), respectively.

output probe beam in the transverse wavevector space appears peaks and valleys due to constructive and destructive interferences. The interference rings will appear, and the number of bright rings is approximately given by the integer of $[\Delta\phi]_{\max}/2\pi$. Figure 4 shows the spatial profile of the probe pulse after propagating through the ionization channel. When the pump beam has not been introduced into the solution, the beam remains the Gaussian profile with larger radius and emissive angle, and no ring can be observed. As the pump energy is increased to 10 μJ, the corresponding peak power is about 200 MW, larger than $P_{\rm cr}$, the plasma channel is formed and two diffraction ring can be observed. When the pump energy increases to 20 μJ, the channel size and plasma density can induce the larger phase shifts, and so four diffraction rings can be observed. However, when the pump energy continually increases to 35 μJ, a single input beam typically can be broken into several optical filaments, and the multi-ionizaiton channel is formed, and then the probe bam will be split into several beams.

The SHG-FROG technique is employed to obtain the spectral amplitude and phase of the probe pulse. As shown in Fig. 5, the SHG-FROG and retrieved envelope phase traces and the power spectra indicate that the probe pulses are greatly modulated with increasing the pump energy, which results in the spectral broadening and the multiple pulse generation. Figures 5 (a)—(c) show a typical SHG-FROG trace, associated retrieved envelope phase trace, and the power spectrum without the pump beams, and the retrieved envelope phase trace indicates a small amount of phase modulation owing to the dispersion of the solution. As the pump energy is increased to 10 μJ, in comparison with the original probe pulse, the SHG-FROG trace in Fig. 5(d) shows that the probe pulses are broadened, and the retrieved envelope phase trace in Fig. 5(e) and the power spectrum in Fig. 5(f) indicate the spectral broadening and multiple pulse formation. As the pump energy increases, the plasma gradient as well as the plasma density will increase. When the probe beam propagates in the ionization channel, the induced self modulation instability (SMI)[20] can cause the break-up of the probe pulses (as shown in Figs. 5(g) and (h)), and the plasma-induced self phase modulation results in the spectral broadening and modulation (as shown in Figs. 5(f) and (i)). When the pump energy is increased to 20 μJ, due to stronger plasma modulation, it is shown that the wider spectrum and more pulses are generated (as shown in Figs. 5(g)—(i)). As the pump energy further increase, the multi-filament will appear, resulting in the break-up of the probe pulse and the rapid decrease of the transmitted probe energy.

In conclusion, the recorded ring patterns from the pump-probe longitudinal diffractometry show that the electronic density gradient in the transverse domain and the size of the plasma channel are functions of the pump energy. SHG-FROG traces indicate that the probe pulses can be broadened and modulated as the pump energy increases, and the further increasing pump energy results in the formation of multiple pulses and multi-filament. The spatiotemporal characteristics will help us to better understand the dynamics of the laser induced plasma and the femtosecond pulse propagating in the plasma channel.

This work was supported by the National Natural Science Foundation of China (No. 10234030 and 10574046), the National Key Project for Basic Research of China (No. 1999075204), the Doctoral Program of High Educa-

tion (No. 20050269011), the Program for New Century Excellent Talents in University (No. NCET-04-0420), the Phosphor Project sponsored by Shanghai Science and Technology Committee (No. 06QH14003), and the Twilight Project sponsored by Shanghai Education Committee (No. 03SG23). Z. Sun is the author to whom the correspondence should be addressed, his e-mail address is zrsun@phy.ecnu.edu.cn.

References

1. X. Wang, M. Krishnan, N. Saleh, H. Wang, and D. Umstadter, Phys. Rev. Lett. **84,** 5324 (2000).
2. A. Ting, C. I. Moore, K. Krushelnick, C. Manka, E. Esarey, P. Sprangle, R. Hubbard, H. R. Burris, R. Fischer, and M. Baine, Phys. Plasmas **4,** 1889 (1997).
3. W. Liu, S. Petit, A. Becker, N. Aközbek, C. M. Bowden, and S. L. Chin, Opt. Commun. **202,** 189 (2002).
4. J. Liu, Z. Duan, Z. Zeng, X. Xie, Y. Deng, R. Li, Z. Xu, and S. L. Chin, Phys. Rev. E **72,** 026412 (2005).
5. F. Courvoisier, V. Boutou, C. Favre, S. C. Hill, and J.-P. Wolf, Opt. Lett. **28,** 206 (2003).
6. J. Kasparian, M. Rodriguez, G. Méjean, J. Yu, E. Salmon, H. Wille, R. Bourayou, S. Frey, Y.-B. André, A. Mysyrowicz, R. Sauerbrey, J.-P. Wolf, and L. Wöste, Science **301,** 61 (2003).
7. M. Rodriguez, R. Sauerbrey, H. Wille, L. Wöste, T. Fujii, Y.-B. André, A. Mysyrowicz, L. Klingbeil, K. Rethmeier, W. Kalkner, J. Kasparian, E. Salmon, J. Yu, and J.-P. Wolf, Opt. Lett. **27,** 772 (2002).
8. X.-J. Fang and T. Kobayashi, Appl. Phys. B **77,** 167 (2003).
9. A. Ting, K. Krushelnick, H. R. Burris, A. Fisher, C. Manka, and C. I. Moore, Opt. Lett. **21,** 1096 (1996).
10. B. E. Lemoff, G. Y. Yin, C. L. Gordon III, C. P. J. Barty, and S. E. Harris, Phys. Rev. Lett. **74,** 1574 (1995).
11. W. L. Kruer, Phys. Plasmas **7,** 2270 (2000).
12. K. A. Tanaka, R. Kodama, H. Fujita, M. Heya, N. Izumi, Y. Kato, Y. Kitagawa, K. Mima, N. Miyanaga, T. Norimatsu, A. Pukhov, A. Sunahara, K. Takahashi, M. Allen, H. Habara, T. Iwatani, T. Matusita, T. Miyakosi, M. Mori, H. Setoguchi, T. Sonomoto, M. Tanpo, S. Tohyama, H. Azuma, T. Kawasaki, T. Komeno, O. Maekawa, S. Matsuo, T. Shozaki, K. Suzuki, H. Yoshida, T. Yamanaka, Y. Sentoku, F. Weber, T. W. Barbee, Jr., and L. DaSilva, Phys. Plasmas **7,** 2014 (2000).
13. E. Esarey, P. Sprangle, J. Krall, and A. Ting, IEEE J. Quantum. Electron. **33,** 1879 (1997).
14. S.-Y. Chen, G. S. Sarkisov, A. Maksimchuk, R. Wagner, and D. Umstadter, Phys. Rev. Lett. **80,** 2610 (1998).
15. R. Zgadzaj, E. W. Gaul, N. H. Matlis, G. Shvets, and M. C. Downer, J. Opt. Soc. Am. B **21,** 1559 (2004).
16. S. P. Le Blanc and R. Sauerbrey, J. Opt. Soc. Am. B **13,** 72 (1996).
17. P. E. Young and P. R. Bolton, Phys. Rev. Lett. **77,** 4556 (1996).
18. S. P. Nikitin, T. M. Antonsen, T. R. Clark, Y. Li, and H. M. Milchberg, Opt. Lett. **22,** 1787 (1997).
19. V. I. Berzhiani, S. M, Mahajan, Z. Yoshida, and M. Pekker, Phys. Rev. E **65,** 046415 (2002).
20. K. Nakajima, D. Fisher, T. Kawakubo, H. Nakanishi, A. Ogata, Y. Kato, Y. Kitagawa, R. Kodama, K. Mima, H. Shiraga, K. Suzuki, K. Yamakawa, T. Zhang, Y. Sakawa, T. Shoji, Y. Nishida, N. Yugami, M. Downer, and T. Tajima, Phys. Rev. Lett. **74,** 4428 (1995).